

Spatial and temporal patterns of nonvolcanic tremor along the southern Cascadia subduction zone

Devin C. Boyarko¹ and Michael R. Brudzinski¹

Received 1 September 2008; revised 21 August 2009; accepted 6 October 2009; published 13 August 2010.

[1] Episodic tremor and slip (ETS), the spatial and temporal correlation of slow slip events monitored via GPS surface displacements and nonvolcanic tremor (NVT) monitored via seismic signals, is a newly discovered mode of deformation thought to be occurring downdip from the seismogenic zone along several subduction zone megathrusts. To provide overall constraints on the distribution and migration behavior of NVT in southern Cascadia, we apply a semiautomated location algorithm to seismic data available during the EarthScope Transportable Array deployment to detect the most prominent pulses of NVT and invert analyst-refined relative arrival times for source locations. In the processing, we also detect distinct and isolated bursts of energy within the tremor similar to observations of low-frequency earthquakes in southwest Japan. We investigate in detail eight NVT episodes between November 2005 and August 2007 with source locations extending over a 650 km along-strike region from northern California to northern Oregon. We find complex tremor migration patterns with periods of steady migration (4–10 km/d), halting, and frequent along-strike jumps (30–400 km) in activity. The initiation and termination points of laterally continuous tremor activity appear to be repeatable features between NVT episodes which support the hypothesis of segmentation within the ETS zone. The overall distribution of NVT epicenters occur within a narrow band primarily confined by the surface projections of the 30 and 40 km contours of the subducting plate interface. We find as much as 50 km spatial offset from the updip edge of the tremor source zone to the downdip edge of the thermally and geodetically defined transition zone, which may inhibit ETS from triggering earthquakes further updip. Intriguingly, NVT activity is spatially anticorrelated with local seismicity, suggesting the two processes are mutually exclusive. We propose that the transition in frictional behavior coupled with high pore fluid pressures in the ETS zone favor tremor generation instead of regular interplate seismicity and frequent ETS produces a semicontinuous relaxation of strain within the overriding and subducting plates that further inhibit seismogenesis surrounding the ETS source region.

Citation: Boyarko, D. C., and M. R. Brudzinski (2010), Spatial and temporal patterns of nonvolcanic tremor along the southern Cascadia subduction zone, *J. Geophys. Res.*, 115, B00A22, doi:10.1029/2008JB006064.

1. Introduction

[2] Along the plate interface of subduction fault systems, the frictional response of the fault is characterized by velocity-weakening (stick-slip) behavior in the shallow seismogenic zone with a transition to velocity-strengthening (stable-sliding) behavior with increasing depth. Recently, geodetically derived slow slip events exhibiting trenchward surface displacements reminiscent of megathrust earthquakes, but with source durations ranging from weeks to years rather than seconds to minutes, have been detected within the expected transitional zone at depths from 25 to 45 km [e.g., Dragert *et al.*, 2001]. Accompanying many

slip events are emergent, low-amplitude seismic signals enriched in the 2–8 Hz frequency passband and depleted in the 10–20 Hz passband of similar magnitude earthquakes, referred to as nonvolcanic tremor (NVT) [e.g., Obara, 2002].

[3] The coupling of the two phenomena, episodic tremor and slip (ETS), was first reported in northern Cascadia [Rogers and Dragert, 2003], and has subsequently been documented in a variety of similar subduction zones with slow convergence rates of young, warm oceanic crust, notably the Nankai Trough in southwest Japan [e.g., Obara *et al.*, 2004] and the Middle America Trench in southern Mexico [Schwartz and Rokosky, 2007; Payero *et al.*, 2008; M. R. Brudzinski *et al.*, Spatial and temporal patterns of nonvolcanic tremor source locations along the Oaxacan segment of the Mexican subduction zone, submitted to *Journal of Geophysical Research*, 2008]. The processes that control ETS and any possible relationships to updip

¹Department of Geology, Miami University, Oxford, Ohio, USA.

seismogenic processes are yet unresolved; although, it has been suggested that updip stress loading during an ETS episode increases the potential for megathrust failure [e.g., *Dragert et al.*, 2004; *Mazzotti and Adams*, 2004].

[4] Considering that ETS has been identified in the transitional zone of the plate interface, determining the extent of ETS over broader regions has implications for defining the downdip extent of the seismogenic zone. This is particularly important in Cascadia, where subduction of the very young, warm Juan de Fuca plate has resulted in a long megathrust earthquake recurrence interval of 500–600 years [Peters *et al.*, 2007], limiting our knowledge of seismic hazard in an area of significant population. There are also few interplate earthquakes in this region [Oppenheimer *et al.*, 1993; Trehu *et al.*, 2008], making it even more difficult to assess the seismogenic behavior of plate interface. ETS holds the promise of shedding new light on plate interface behavior, particularly as some potential spatial and temporal relationships between ETS and the seismogenic zone are emerging [Brudzinski *et al.*, 2007; Brudzinski and Allen, 2007]. Surface-based geodetic instruments can help us to see the direction of motion during ETS and are used to estimate the overall slip distribution for larger slip events [e.g., *Dragert et al.*, 2001; *Melbourne et al.*, 2005; *Szeliga et al.*, 2008], but one cannot yet decipher the detailed evolution of slip in space or time with this data. Comparisons of slow slip events and NVT in Cascadia suggest the two phenomena are closely linked and that one could be used as a proxy for the other [Aguiar *et al.*, 2007]. Therefore, we propose to use precise NVT source locations as a means to evaluate the intricate details of slow slip migration, directionality, and segmentation.

[5] Owing to the wealth of geodetic and seismic observatories in Washington and Vancouver Island, ETS in northern Cascadia has been the subject of numerous studies over the last half-decade [e.g., *McCausland et al.*, 2005; *Kao et al.*, 2005; *La Rocca et al.*, 2005; *Kao et al.*, 2006; *Royle et al.*, 2006; *Wech and Creager*, 2008; *Kao et al.*, 2009]. A few additional studies in other parts of the subduction zone began to find ETS was also prevalent in southern Cascadia [e.g., *Szeliga et al.*, 2004; *McCausland et al.*, 2005; *Brudzinski and Allen*, 2007], and the arrival of EarthScope instrumentation at the end of 2005 provided new opportunities to examine ETS in this region in detail. Our study is the first to attempt to acquire NVT source locations throughout the southern half of the Cascadia margin to characterize along-strike migration patterns over a broader region of this subduction zone (Figure 1). We identify eight NVT episodes between November 2005 and August 2007 using a semiautomated location routine to detect the most prominent bursts within the tremor waveforms and invert analyst-confirmed relative arrival times for source locations. Although previous processing of GPS data for transient motion is limited in this region [*Holtkamp and Brudzinski*, 2010], it suggests that NVT is concurrent with slow slip, and hence represents ETS. NVT source locations occur throughout the full extent of southern Cascadia, but are intriguingly anticorrelated with local seismicity. We compare the spatial distribution of tremor epicenters to the plate interface depth, temperature, and coupling structure and find that tremor is offset inland from the downdip edge of the thermally and geodetically defined transition zone.

We also uncover an assortment of tremor migration behaviors, which appear to conform to recently defined ETS segmentation boundaries.

2. Data and Methods

[6] Nonvolcanic tremor is typically characterized by emergent, low signal-to-noise ratio arrivals, so exact arrival times are often ambiguous. Previous studies of NVT in Cascadia have employed grid searches for correlation of envelope seismograms as a means of locating similar signals at multiple stations [e.g., *Kao and Shan*, 2004; *Wech and Creager*, 2008]. This approach has worked well in areas with close station spacing and hence similar waveforms from station to station. We initially applied the cross-correlation location technique of *Obara* [2002] for southern Cascadia [Boyarko and Brudzinski, 2007], but we found the wider (~80 km) station spacing degraded the waveform similarity and it was common for multiple widely spaced sources of NVT to be active synchronously (Figure 2), further confusing the correlation algorithm. The resulting source locations were artificially spread as far as the station coverage and had large uncertainties. Based on these preliminary results, we decided instead to analyze individual waveforms more carefully to focus on times of the largest amplitude tremor, verify waveform similarity and coherence, and confirm source locations are consistent with observed seismograms.

[7] To this end, we have developed a semiautomated source location approach and applied it to the eight most prominent NVT episodes that occurred throughout the southern half of the Cascadia subduction zone between November 2005 and August 2007. This time period was chosen as it corresponds to the deployment of the EarthScope USArray Transportable Array in this region, significantly increasing the station density. Other data for this study came from the regional stations of the Pacific Northwest Seismic Network (PNSN), Berkeley Digital Seismograph Network (BDSN), Global Seismograph Network (GSN), Plate Boundary Observatory (PBO), and the Oregon Array for Teleseismic Study (OATS). The data used was collected from the IRIS DMC and was recorded on either three-component broadband or vertical-component short-period instruments.

[8] The semiautomated location routine is composed of three stages. First, we apply the automated NVT scanning method of *Brudzinski and Allen* [2007] to all available seismic data to identify the approximate spatial and temporal distribution of tremor activity. Second, for the most active hour on days with tremor activity, we employ an automated algorithm on stacked envelope seismograms to detect distinct bursts of energy with large STA-to-LTA ratios on a subnetwork of stations and pick high signal-to-noise peaks on individual waveforms. All detected arrivals are visually inspected to confirm signal coherence and to perform arrival time adjustment if necessary. The third and final step inverts all sets of relative arrival times for source locations, estimates location uncertainties, and discards poor locations.

2.1. Automated Nonvolcanic Tremor Scanning Method

[9] To provide a spatial and temporal guide to times of the most prominent tremor activity, we first utilize the automated

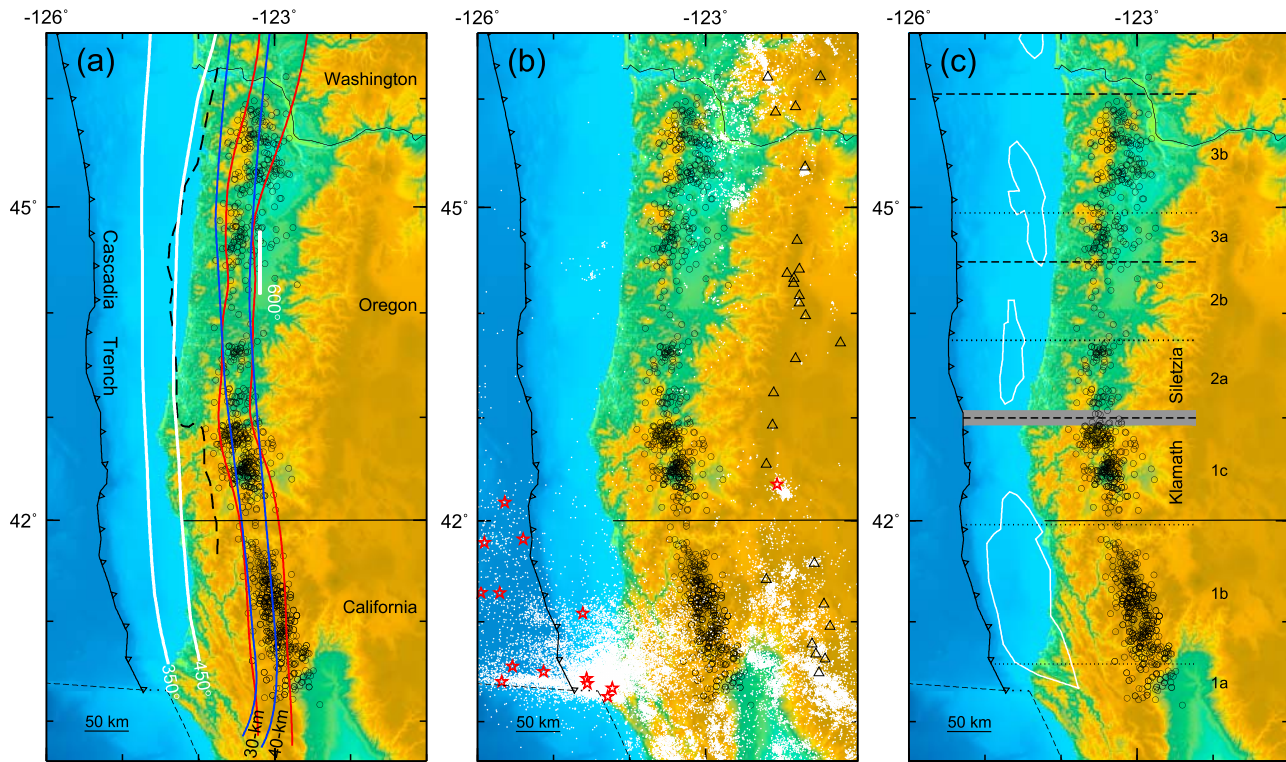


Figure 1. Distribution of southern Cascadia NVT epicenters from eight episodes between November 2005 and August 2007 (black circles). (a) Comparison with interplate thermal, depth, and coupling contours. The 350°C–450°C and 600°C thermal contours (white curves) are from Hyndman and Wang [1995] and Bostock *et al.* [2002], respectively. The 30 and 40 km surface projections of the subducting plate interface are from McCrory *et al.* [2004] (blue curves) and Audet *et al.* [2010] (red curves). Dashed line represents the downdip edge of long-term interplate coupling from Burgette *et al.* [2009]. (b) Comparison with local seismicity (white circles) from the Advanced National Seismic System (ANSS) earthquake catalog. Large seismicity ($M_w > 6$) are plotted as red stars. Open triangles correspond to Cascade volcanic centers. The colored base map shows topography and bathymetry. (c) Interpretation of segmentation throughout the ETS zone. The dashed lines correspond to long-term segmentation boundaries identified by Brudzinski and Allen [2007]. The dotted lines correspond to subsegment boundaries found during the 2 years studied. Shaded area corresponds to the approximate boundary between the Klamath and Siletzia geologic terrains. Black polygons depict locations of offshore fore-arc basins from Wells *et al.* [2003] thought to represent seismogenic zone asperities.

NVT scanning method of Brudzinski and Allen [2007], which begins by removing the instrument response from an hour long seismogram, band-pass filtering at 2–6 Hz, taking the absolute value and calculating envelope seismograms. A time series is calculated from the mean amplitude of filtered envelope seismograms for each hour recorded at individual stations. After a moving average and normalization, large peaks rising above background noise at 99% confidence are identified as periods during which NVT dominates (Figure S1).¹ Stations with similar timing of tremor activity were taken to represent the primary network on which further analysis is performed.

[10] We characterize patterns of tremor in space and time by analyzing the most active nighttime hour for every day of a given NVT episode. The most active hour of each day is chosen by calculating the mean amplitude for every nighttime hour for individual stations and identifying when

tremor activity is maximized throughout the primary network [Brudzinski and Allen, 2007]. As discovered in our preliminary study attempting to use cross correlation to determine source locations [Boyarko and Brudzinski, 2007], we document many instances where multiple source regions of tremor are synchronously active. So for each hour analyzed, all seismic waveforms of the primary network are visually inspected to distinguish network subsets which display a coherent, synchronous tremor source (Figure 2).

2.2. Automated Signal Detection Algorithm

[11] Once an hour and subnetwork have been selected for further analysis, we prepare the waveforms for automated processing. We help clarify the bursts of energy from station to station by smoothing the hour long envelope seismograms with a 0.06 low-pass filter and then stacking all components of envelope seismograms. This station stacking procedure is performed for two reasons: (1) the most prominent S wave arrivals are sometimes found on different components depending on the station back azimuth and

¹Auxiliary materials are available in the HTML. doi:10.1029/2008JB006064.

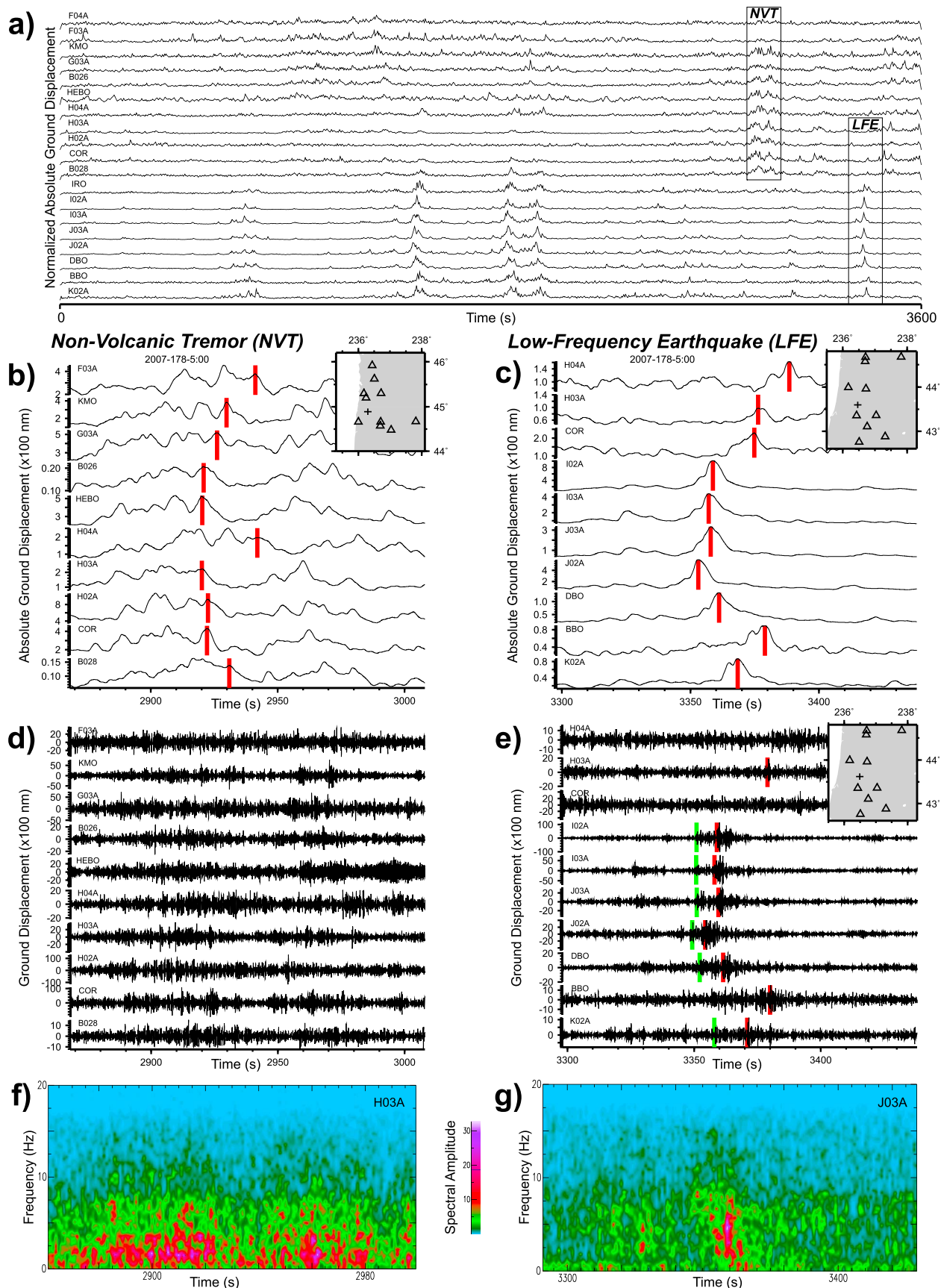


Figure 2

incidence angle and (2) the average signal-to-noise for any individual component is 2.6, whereas the average signal-to-noise ratio for the stacked components is 3.5.

[12] To identify when tremor signals are most active during the hour, we stack all of the subnetwork station envelope seismograms together. Automated processing identifies prominent pulses rising above background noise in this subnetwork activity time series with a ratio of the short-term average (STA, 10 s window) to the long-term average (LTA, 100 s window) greater than 2. For each subnetwork activity peak time, the algorithm selects peaks within 15 s on station envelope waveforms that have signal-to-noise ratios of at least 1.5. We then visually inspect all automated selections to confirm coherent signals with reasonable moveout times representative of a common source, and we adjust the selected time if necessary to best represent the station-to-station relative timing of energy packets. Considering the larger amplitudes on horizontal components and apparent velocity in record sections (Figure 2), all confirmed arrival times are treated as *S* wave arrival times in subsequent location analysis. As indicated earlier, this semiautomated approach is dictated by the emergent nature of NVT, small signal-to-noise ratio arrivals and wide station spacing, but we estimate that the median picking uncertainty is less than 1 s based on evaluation of over 100 waveforms.

2.3. Source Location and Uncertainty Determination

[13] When a coherent NVT burst is confirmed at a minimum of four stations, the relative arrival times are used to invert for a source location using a 1-D regional *S* wave velocity model for central Cascadia [Ludwin *et al.*, 1994]. The source inversion is performed using the computationally efficient ELOCATE algorithm [Hermann, 2004], which produces nominal uncertainties based on incoherence between arrival times. We also recalculated locations many times by randomly adjusting arrival times between -1.0 and 1.0 s to estimate the location uncertainty potentially due to picking error, finding the locations differed on average 3 km in the horizontal direction and 10 km in the vertical direction. In addition, we obtained formal location uncertainty estimates based on bootstrap location reliability [Efron, 1979; Wech and Creager, 2008]. For each event we iteratively remove each station from the input arrival times, one at a time, and search for a location. We interpret the median of the resulting cloud of locations as the source centroid epicenter with an error estimated by the absolute deviation.

[14] To help focus on our best resolved locations in our discussion of patterns in NVT source locations, we only interpret the events with all forms of uncertainty less than 15 km in the horizontal and vertical directions. As with

previous studies of NVT [e.g., Obara, 2002; Wech and Creager, 2008], we seek episodes with regional coherence by rejecting locations that are greater than 30 km distance from any other location during the 4 days before and after. We further limit locations by rejecting cases when the origin time is coincident with origin times found in local earthquake catalogs.

2.4. Spectral Characteristics of Nonvolcanic Tremor

[15] To establish a relationship between nonvolcanic tremor in southern Cascadia and its counterpart to the north, as well as to discriminate NVT signals from regular earthquakes, we calculated the amplitude spectra following the approach of Kao *et al.* [2006] for all NVT and low-frequency earthquakes (LFEs) detected during the 2007 June to August NVT episode and compare them with seismicity reported in the ANSS seismic catalog. NVT, LFE, and earthquake spectra are calculated for *S* wave arrivals for a 10 s window, from 1 s before to 9 s after the catalog arrival, whereas the background noise time segment is taken from a relatively quiet portion away from the signal segment. To make a more meaningful comparison between tremors and earthquakes with different magnitudes, all signals are normalized against the amplitude of background noise at 1 Hz. Finally, frequency spectra of all seismograms from the same type of signal are stacked by taking the median value at each frequency to give the average spectrum curves. In total, 597 NVT, 153 LFE, 30 M_L 0.5–1, 82 M_L 1–1.5, 31 M_L 2.5–3.5, and 604 background noise seismograms were stacked to produce the spectrum curves in Figure 3.

[16] The spectra of nonvolcanic tremor show maximum amplitudes in a narrow frequency band from 1 to 4 Hz, followed by a progressive decay in amplitude with increasing frequency (4–20 Hz). At frequencies below 1 Hz, the tremor spectra show relatively larger amplitudes when compared with the spectra of lower-magnitude earthquakes. The spectral characteristics of nonvolcanic tremor in southern Cascadia reflect those seen in northern Cascadia [Kao *et al.*, 2006]. Additionally, within rather quiescent periods of tremor activity we observe distinct and isolated signals interpreted to be low-frequency earthquakes (see section 7). The spectra of low-frequency earthquakes parallels that of tremor which suggests the two phenomena are genetically related. Local seismicity (M_L 0.5–1) exhibit comparable amplitudes in the NVT frequency passband, but differ markedly in that they maintain larger amplitudes at higher frequencies. The spectra of larger magnitude seismicity ($M_L > 1$) follow a similar trend, but with overall larger amplitudes, which suggests there is an underlying difference in the source process of NVT/LFE and regular seismicity. Considering

Figure 2. Semiautomated detection of synchronous NVT and LFE source regions in northern and central Oregon during 1 h beginning at 0500 GMT on 27 June 2007. (a) Envelope seismograms where all available components have been stacked together at each station. (b) Expanded view of the subnetwork box labeled NVT in Figure 2a with analyst-confirmed picks marked with vertical red lines. Inset shows the epicenter (cross) obtained by inversion of relative arrival times. (c) Same as Figure 2b but for the subnetwork labeled LFE. (d and e) Single component raw seismograms of Figures 2b and 2c band-pass-filtered from 2 to 6 Hz. Absolute *P* wave and *S* wave arrivals in Figure 2e are marked with vertical green and red lines, respectively. Inset shows the epicenter (cross) obtained by inversion of absolute arrival times. (f) Spectrogram of station H03A from Figure 2d high-pass-filtered at 1 Hz; color scale denotes frequency intensity. (g) Spectrogram of station J03A from Figure 2e.

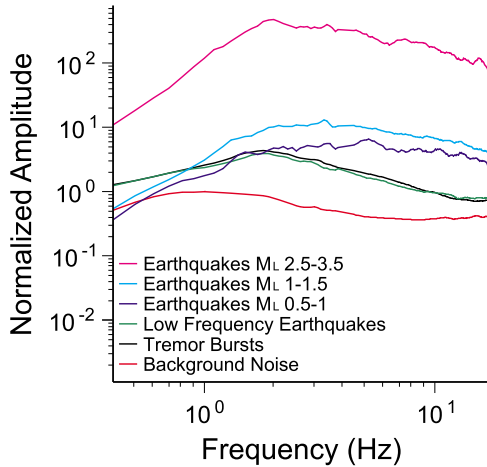


Figure 3. Spectral characteristics of NVT, LFE, local seismicity, and background noise. All of the collected waveforms are calibrated to the same short-period sensor and gain range. To ensure frequency spectra are representative of source characteristics with minimal path effects, we only use seismograms with high signal-to-noise ratios recorded within 50 km of the earthquake or tremor epicenters. The spectrum of NVT shows maximum amplitudes in the frequency band of 1–4 Hz, followed by a gradual decay in amplitude with increasing frequency. The spectrum of LFE is remarkably similar to NVT which suggests they share a similar source process. The spectra of local seismicity do not exhibit a rapid decay in amplitude with increasing frequency regardless of magnitude.

that tremor and earthquakes are thought to represent different frictional regimes [e.g., Yoshida and Kato, 2003], this result is not unexpected.

3. Geographic Distribution of Nonvolcanic Tremor Sources

[17] The epicentral locations of all well-constrained tremors between the November 2005 and August 2007 determined with our semiautomated processing of NVT reveal a nearly continuous belt-like distribution 650 km in length along the southern half of the Cascadia subduction zone (Figure 1). The northern limit of the tremor epicenters from our study terminate near the Oregon-Washington border, whereas, the southern limit coincides with the edge of the subducting Gorda plate in northern California ($\sim 40.25^\circ\text{N}$). The average width of the tremor belt is ~ 40 km throughout northern California and Oregon. From north to south, the center of the curvilinear belt of tremor gradually increases in distance from the coastline (from ~ 50 to ~ 100 km), but has a more variable relationship to distance from the trench (between ~ 150 and ~ 200 km). Before we interpret individual tremor episodes in section 4, we begin by comparing this overall distribution of tremor epicenters with patterns in slab morphology, temperature, and local seismicity.

3.1. Comparison With Slab Depth Structure

[18] Since NVT has been proposed to represent shear failure along the plate interface [e.g., Shelly et al., 2006; Ide et al., 2007], we investigate the potential relationship

between the distribution of tremor epicenters in southern Cascadia with the depth of the subducting plate interface. The two most current models of the subducting plate interface, McCrory et al. [2004] and Audet et al. [2010], were developed using independent data sets that lead to some differences in depth structure. The McCrory et al. model was developed utilizing local earthquake hypocenters, teleseismic travel time data, and reflection and refraction transects, while the Audet et al. model was developed utilizing teleseismic body wave data to construct receiver functions that identify the plate interface at 20–40 km depth.

[19] With respect to the depth contours from the McCrory et al. [2004] model, the distribution of tremor epicenters throughout most of southern Cascadia are bounded by the surface projections of the 30 and 40 km contours of the subducting plate interface, with the exception of two divergences in northern Oregon and northern California where the tremor sources occur over deeper parts of the plate interface (Figure 1a). However, the 30 and 40 km contours from the Audet et al. [2010] model do account for the eastward trend observed in northern Oregon and remarkably conforms to the curvilinear distribution of tremor epicenters in southern Oregon. Yet, the Audet et al. model is also unable to account for the eastward trend of NVT epicenters in northern California as they approach the southern edge of the subducting Gorda slab, which suggests the tremor source is either associated with deeper regions of the plate interface near the edge of the slab or there is persistent difficulty in determining the depth of the plate interface in that region. Regardless of the depth model used, nearly all of the reported tremor epicenters in this study occur within a narrow band defined by the 30 and 40 km depth contours of the subducting plate interface, which is comparable to the spatial distribution of tremors reported in northern Cascadia and southwest Japan [Obbara, 2002; Kao et al., 2005; Wech and Creager, 2008].

[20] As seen in previous studies of northern Cascadia, our results display a wide depth distribution where hypocenters locate throughout the overriding plate and into the subducting plate [Kao et al., 2005; McCausland et al., 2005; La Rocca et al., 2005; Royle et al., 2006]. Figure 4 shows six cross sections binned per degree latitude to illustrate the along-strike distribution in tremor source depths. While our results suggest southern Cascadia NVT occur within a distributed deformation zone surrounding the plate interface, previous studies in northern Cascadia and southwest Japan using more sophisticated location routines that utilize *P* and *S* wave arrivals reveal tight clustering of tremor sources near the plate interface [Shelly et al., 2006; Shelly et al., 2007a, 2007b; La Rocca et al., 2009]. Considering our depth uncertainties using *S* wave envelopes alone, we believe it is premature to interpret that southern Cascadia NVT occurs over a distributed deformation zone or as focused interplate deformation.

3.2. Comparison With Plate Interface Thermal Structure

[21] The thermally defined seismogenic and transition zones traditionally correspond to 100°C – 350°C and 350°C – 450°C on the plate interface and are often used to represent the downdip rupture limit of great subduction zone

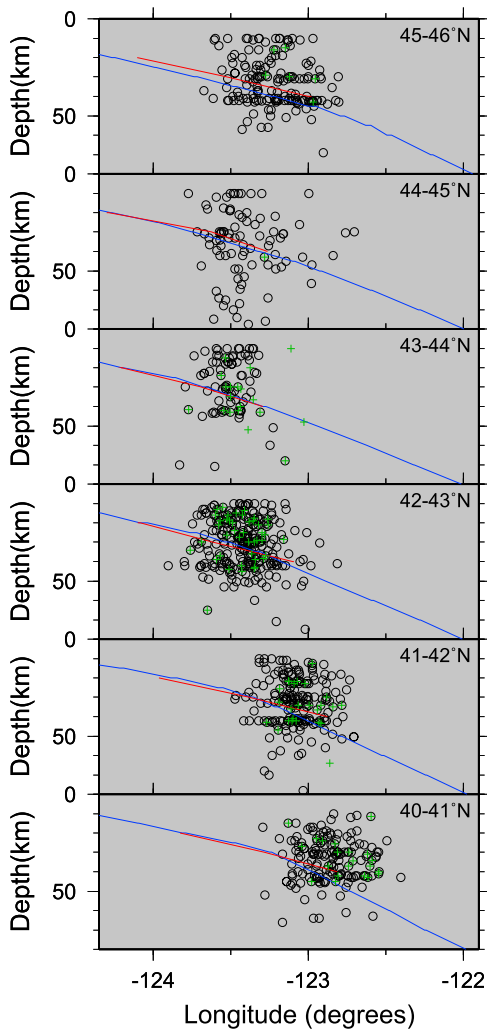


Figure 4. Cross sections illustrating the depth distribution of NVT (black circles) and LFEs (green crosses), divided per degree latitude. The blue and red curves correspond to the plate interface from McCrory *et al.* [2004] and Audet *et al.* [2010]. Depth uncertainties up to ± 15 km inhibit interpretation of whether southern Cascadia NVT and LFE occur over a distributed deformation zone or as focused interplate deformation.

earthquakes. Numerical thermal modeling and elastic dislocation modeling of interseismic geodetic data are in good agreement that the extension of the primary locked zone of the plate interface throughout the Cascadia subduction zone is located offshore where the slab depth is less than 20 km [Hyndman and Wang, 1993, 1995]. A recent study of tidal and leveling records since 1925 further defines the edge of interseismic coupling in our study region, which is in agreement with the 450°C isotherm through most of Oregon, but the zone of long-term coupling moves inland ~ 30 km within the Klamath terrane in southernmost Oregon [Burgette *et al.*, 2009] (Figure 1a).

[22] Figure 1a shows the spatial relationship between the thermal structure of the plate interface as defined by Hyndman and Wang [1995] in relation to the belt-like distribution of tremor epicenters; in central Oregon, the thermal

contour of 600°C is inferred from a similar thermal model [Bostock *et al.*, 2002]. The updip extent of southern Cascadia tremor epicenters is offset ~ 50 km in relation to the downdip extent of the thermal transition zone, placing tremor in a region where the interplate thermal structure is $\sim 550^{\circ}\text{C}$ – 600°C . In contrast, the distribution of northern Cascadia tremor epicenters borders the downdip extension of the thermal transition zone, placing tremor where the interplate thermal structure is $\sim 450^{\circ}\text{C}$ – 500°C [Kao *et al.*, 2005; Wech and Creager, 2008].

[23] Further diversity exists within and between similar warm end-member subduction zones when comparing the thermal regime and the source zone of ETS. NVT in southwest Japan displays along-strike variations where sources occur over temperatures ranging from 400°C to 500°C [Yoshioka and Murakami, 2007]. Additionally, in the Oaxacan segment of the Middle America Trench, NVT occur where the expected interplate temperatures range from $\sim 450^{\circ}\text{C}$ to 550°C (Brudzinski *et al.*, submitted manuscript, 2008). The disparity in temperatures where NVT occurs across several subduction zones suggests that temperature alone does not appear to be a fundamental control on tremor generation. This complements a similar conclusion recently reached for slow slip events in New Zealand, where events occur at temperatures ranging 100°C – 400°C [McCaffrey *et al.*, 2008].

3.3. Comparison With Local Seismicity

[24] To investigate potential spatial relationships between ETS and earthquakes, we overlay seismicity from the Advanced National Seismic System (ANSS) earthquake catalog from 1898 to 2009 (available at <http://www.ncedc.org/anss>, accessed 18 February 2009) on our map of tremor locations from the NVT episodes between November 2005 and August 2007 analyzed in this study. Despite the fact that earthquake density is irregular along the margin, we notice a distinct trend where earthquakes are generally absent within the tremor band (Figure 1b). This is particularly striking in areas of increased seismicity like northern California, and to a lesser degree in northern Oregon, with the former demonstrating how seismicity terminates at both the eastern and western margins of the tremor locations. Cross sections through these two regions illustrate how both seismicity associated with the dipping slab and that within the overlying crust come to an abrupt halt where tremor is focused (Figure 5, left). While some of the shallower inland seismicity is likely due to structures associated with the arc volcanoes, midcrustal earthquakes extend ~ 70 km west of the Cascades before dying out at the edge of the tremor region. Finally, we construct histograms of the number of earthquakes and tremor bursts that correspond to these cross sections to verify the activity is truly anticorrelated (Figure 5, right). We find in each case that earthquake activity decreases precisely as the tremor activity increases, and cases in northern California show the maximum in tremor activity correspond to the minimum in earthquakes activity and, thus the spatial distribution of nonvolcanic tremor appears to be inversely proportional to local seismicity, which suggests these two processes occur exclusive of one another.

[25] An important issue that needs to be evaluated regarding the inversely proportional relationship between nonvolcanic tremor and seismicity in northern California is

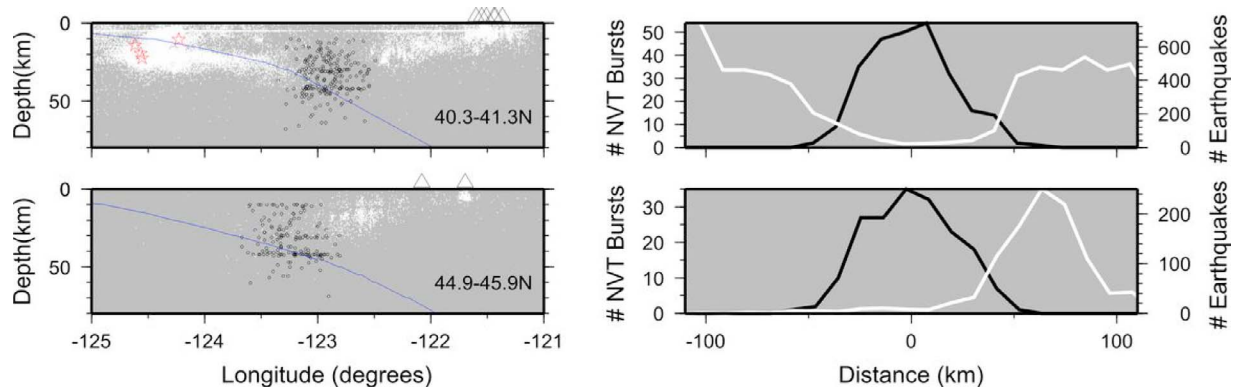


Figure 5. Spatial distribution of NVT with respect to local seismicity. (left) West-to-east cross sections illustrating the spatial anticorrelation of NVT (black circles) and local seismicity (white circles). Plate interface is from McCrory *et al.* [2004] (blue curve). Holocene volcanoes within the specified latitude ranges are plotted. (right) Smoothed histograms of counts of NVT and seismicity binned per 0.1° longitude corresponding to the latitude ranges in Figure 5 (left).

the inland extent of plate boundary stresses within the subducting Gorda and overriding North America plates. Elevated strain rates within the Gorda plate near the Mendocino Triple Junction and increased levels of intraslab seismicity are products of shear strain accommodation due to the north-northwest push of the Pacific plate. The sense of deformation within the subducting slab changes from strike-slip to normal faulting with increasing depth as the maximum principal stress (σ_1) orientation changes from margin parallel to vertical [Wang and Rogers, 1994], thus one should not expect increasing distance from the triple junction to be the primary cause of diminished levels of intraslab seismicity. Likewise, elevated strain rates within the overlying North America crust near the Mendocino Triple Junction arise from contributions of Gorda–North America convergence, northwest convergence of the Sierra Nevada–Great Valley block, and the north-northwest encroachment of the San Andreas Fault system. Williams *et al.* [2006] isolated the contribution of upper plate strain from the San Andreas Fault and Sierra Nevada–Great Valley block in northern California find that shear induced strain penetrates as far north as 41.5°N and as far east as -122.5°E . Fay and Humphreys [2008] reach a similar conclusion finding that Pacific–North America shear stresses in northern California persist inland from $\sim 1.5 \text{ TN/m}$ on the western margin of the Sierra Nevada block to $\sim 1.1 \text{ TN/m}$ on the eastern margin in the Walker Lane Belt to near zero in central Nevada. Although plate boundary stress and strain gradients in both the subducting and overriding plates are expected to decrease toward the continental interior, we call attention to the fact that seismicity levels decrease from east to west in both northern California and northern Oregon, precisely where the tremor zone occurs. It would seem exceedingly fortuitous that tremor just happens to occur in a zone where stresses from plate boundary and plate interior processes drop below a seismogenic threshold, and instead suggests that some physical mechanism associated with the onset of ETS activity likely contribute to the observed pattern of deformation.

[26] Another anticorrelation between earthquakes and tremor has been reported on Vancouver Island [Kao *et al.*,

2009]. In that case, a persistent gap in tremor locations is observed where the epicenters of the only two large (magnitude > 6) crustal earthquakes have occurred on Vancouver Island over the last ~ 150 years. This has led to two hypotheses: (1) the lack of tremors indicates stress is not being released via ETS such that stress is accumulating toward the next large crustal earthquake (tremor controls where seismicity occurs) or (2) the occurrence of large earthquakes in the relatively recent past significantly reduced crustal stress and/or pore fluid pressure, thereby inhibiting tremor activity in this region for some period of time (seismicity controls where tremor occurs). Although there are no comparable large crustal earthquakes near the southern end of the subduction zone (stars in Figure 1b), one could argue along the lines of the second hypothesis such that smaller earthquakes are still controlling the presence of tremor. However, this argument does not work in northern Oregon, as there is no seismicity to the west of the tremor band to inhibit its occurrence, or in southern Oregon where there is no prominent seismicity on either side, yet the tremor band maintains a similar width through this region.

[27] Instead, we believe our results support the first hypothesis that ETS can act as an inhibitor of seismicity. We interpret this relationship in the context of stress domain analysis associated with the subduction thrust fault. Based on Coulomb stress modeling, slow slip events reduce the average value of stress on the fault while increasing stress at both the updip and downdip ends of the fault and reducing stress both above and below the fault [Dragert *et al.*, 2004]. So while interseismic coupling is expected to promote strain accumulation around the plate interface, repeated ETS episodes and frequent inter-ETS activity [e.g., Kao *et al.*, 2006; Wang *et al.*, 2008; Wech and Creager, 2008] may result in a semicontinuous relaxation of strain within the overriding and subducting plates near the ETS source region. Such a scenario may account for the minimal levels of seismicity on and off the fault as the stress failure threshold in the near field is subdued.

[28] It is important to note that increased rates of microseismicity occur in conjunction with positive Coulomb

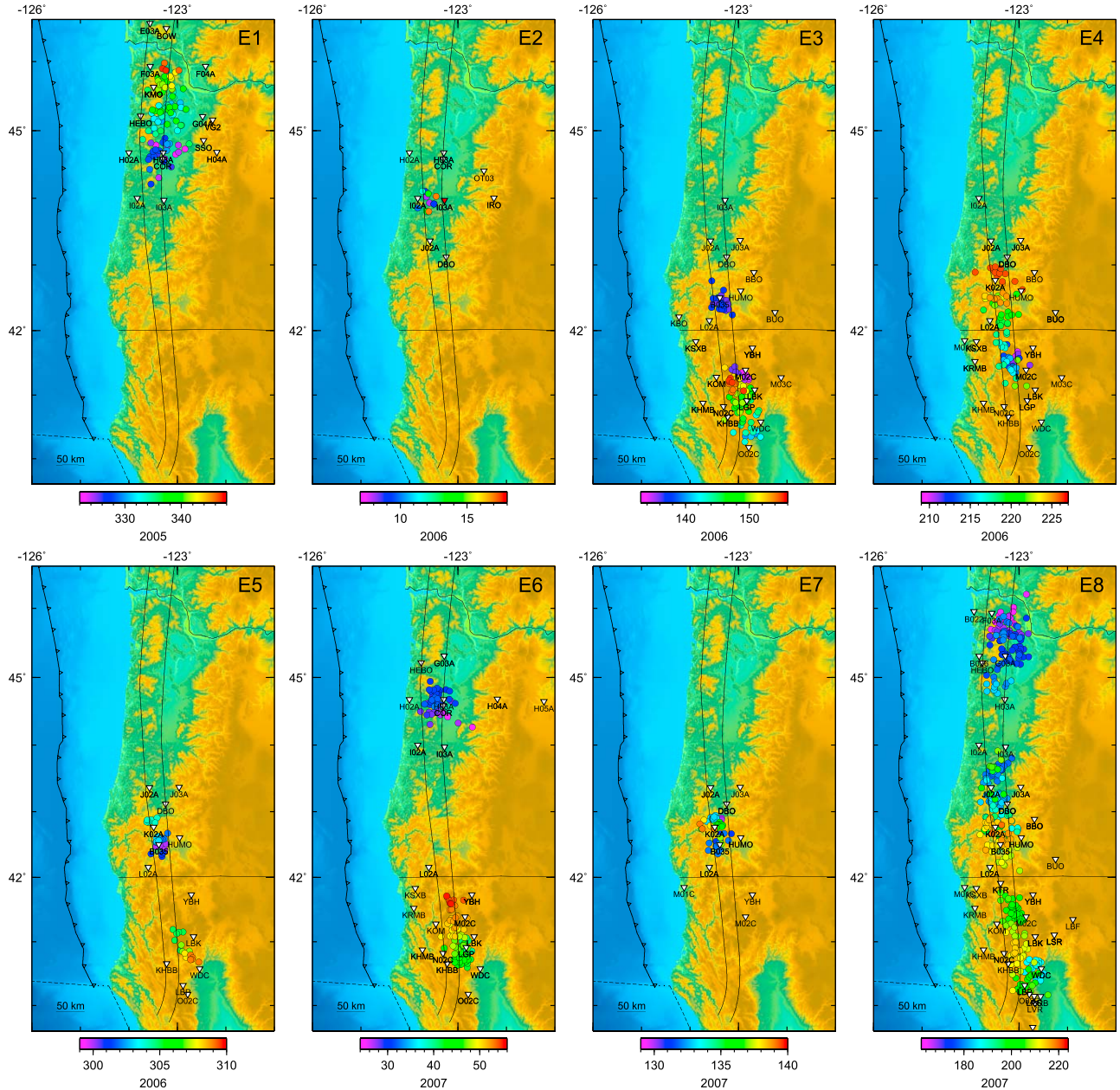


Figure 6. Geographic distribution and migration of individual NVT episodes. NVT epicenters are circles with color indicating day of the year. Black curves are the 30 and 40 km projections of the subducting plate interface from McCrory *et al.* [2004]. The annotated, inverted white triangles show the seismic stations used to determine source locations. The red station in E2 was installed near the tail end of the episode such that data were only available for a few days.

stress changes following several slow slip events on Kilauea volcano, Hawaii, suggesting that under different circumstances slow slip could be an effective earthquake triggering mechanism [e.g., Segall *et al.*, 2006]. Similar links between slow slip and temporal increases in seismicity have been observed in Boso, Japan [e.g., Ozawa *et al.*, 2007], northern New Zealand [Delahaye *et al.*, 2009], and the Salton Trough [Lohman and McGuire, 2007]. However, there is no evidence for nonvolcanic tremor during any of these slow slip events, which is in contrast to subduction zone ETS like in Cascadia where slow slip is accompanied by nonvolcanic

tremor with no reported temporal increase in microseismicity. In fact, a simple comparison with local seismicity rates in the ANSS catalog finds no clear increases associated with our analyzed tremor episodes.

[29] So regardless of whether slow slip is ongoing or not, it appears the physical process that allows for tremor to occur in a region also prevents earthquake rupture in the same region. We suggest that the combination of high pore fluid pressures and the transition in frictional behavior from velocity weakening to velocity strengthening, favors the generation of tremor instead of regular seismicity. Several

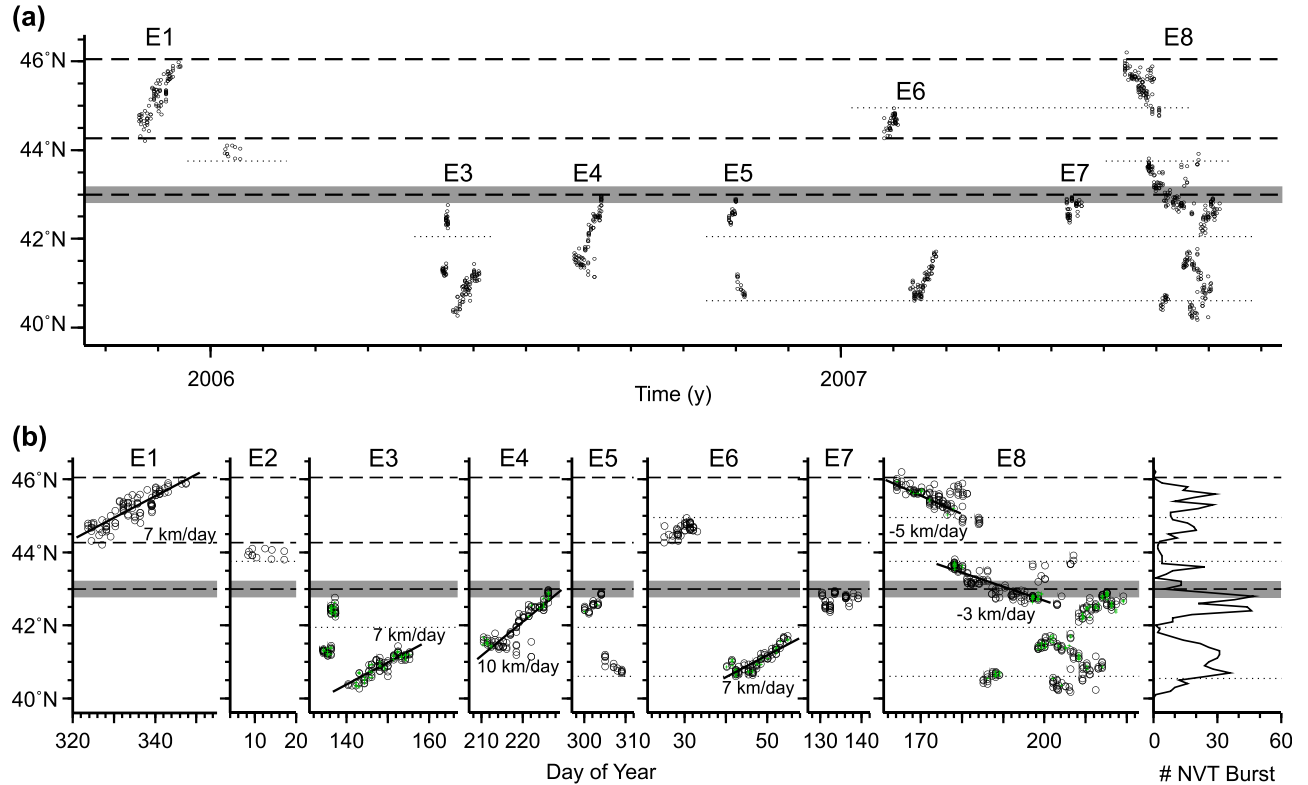


Figure 7. Space-time plots of NVT (black circles) and LFEs (green crosses). E1–E8 correspond to NVT episodes shown in Figure 6. Horizontal lines are segmentation boundaries from Figure 1c. (a) Full time plots between November 2005 and August 2007. (b) Zoomed in views of each episode plotted with time in day of year. Annotated sloped lines denote average rates for periods of steady migration. Also shown is cumulative along-strike NVT and LFE frequency histogram binned per 0.1° latitude and smoothed.

independent lines of evidence suggest that like regular seismicity, to initiate slip instabilities at transition zone depths, very low effective stress on the plate interface is necessary. These include observations of increased NVT activity excited by very small stress perturbations (~ 0.4 bar) due to passing seismic waves [e.g., Rubinstein *et al.*, 2007, 2009] and solid earth and ocean tidal (~ 0.1 bar) fluctuations [e.g., Rubinstein *et al.*, 2008], as well as theoretical models that need to rationalize the large spatial dimension and short (~ 1 year) recurrence of slow slip [Liu and Rice, 2005, 2007]. Effective stress, defined as the normal stress minus the pressure from fluids in rock pores, is probably low due to high pore pressure, rather than low normal stress, and likely results from dehydration of the subducting plate. Near-lithostatic pore fluid pressure in the oceanic crust beneath the origin of episodic tremor and slip is supported by seismic velocity analysis from Cascadia [Audet *et al.*, 2009, 2010], as well as results from southwest Japan [Kodaira *et al.*, 2004; Shelly *et al.*, 2006; Matsubara *et al.*, 2009] and Mexico [Song *et al.*, 2009]. Frictional models that incorporate the tendency for pore volume to increase with shear, decreasing pore pressure and increasing frictional resistance, can explain how slip instabilities nucleate but become quenched before reaching fast earthquake slip speeds, as pore pressures drop faster than they can be replenished [Segall and Rice, 1995]. Audet *et al.* [2010] propose a stochastic model for the generation of ETS where the occur-

rence and recurrence of propagating slow slip and NVT are explained by episodic pore fluid pressure build up and fluid release across the plate boundary.

4. Nonvolcanic Tremor Migration Patterns

[30] We determine migration patterns by tracking tremor locations over the time span of each episode (E1–E8; Figures 6 and 7). We find several types of NVT migration patterns (steady, halting, and jumping) in our study region that have also been documented in northern Cascadia [cf. Kao *et al.*, 2007]. Table 1 summarizes the migration behaviors observed in all eight of the NVT episodes analyzed in this study.

[31] The first type of behavior is “steady” migration which refers to a continuous unidirectional source propagation via clusters of locations migrating at relatively uniform rates. A prime example of steady migration is observed during episode E1 (Figures 6 and 7). Tremor activity initiates in central Oregon (44.5°N) and propagates unidirectionally to the north at an average rate of 7 km/d until activity ceases near the Oregon–Washington border (46°N). We find several episodes propagate unidirectionally, although there appears to be no preference for directionality between episodes occurring in similar locations during the 2 year period we examined. For cases with at least 10 days of spatially and temporally continuous activity, average migration rates

Table 1. Summary of Nonvolcanic Tremor Episodes in Southern Cascadia

Event	Starting Date	Total Duration (days)	Region ^a	Cumulative Length of Activity (km)	Along-Strike Extent (km)	Migration Pattern ^b
E1	19 Nov 2005	44	3a, 3b	180	180	N
E2	6 Aug 2006	9	2b	30	30	H
E3	14 May 2006	30	1a, 1b, 1c	200	270	N, H, J, T
E4	29 Jul 2006	16	1b, 1c	130	130	N, S, H, B
E5	27 Oct 2006	9	1b, 1c	120	250	N, S, J
E6	24 Jan 2007	24	1b, 3a	210	500	N, H, J
E7	10 May 2007	9	1c	80	80	H
E8	13 Jun 2007	57	1a, 1b, 1c, 2a, 3b	610	680	N, S, H, J, B, T

^aRegions are defined by segmentation boundaries in Figure 1c.

^bN, northward; S, southward; H, halting; J, jumping; B, bifurcation; T, terminal convergence.

range from 3 to 10 km/d based on a simple linear fit, which are similar to many previous studies of NVT [e.g., Schwartz and Rokosky, 2007]. However, the other behaviors discussed below document how migration rates can be quite variable during a given episode.

[32] The second type of behavior is “halting” migration which refers to an along-strike propagation of sources when the migration rate decreases until the tremor source region becomes relatively stationary. Several examples of halting migration are observed, including a clear case at the end of episode E3 (Figure 7). The average migration velocity of this episode is 7 km/d, but it is characterized by an initial steady northward propagation which transitions into a halting phase where activity remains relatively stationary at ~41.3°N for 5 days. We also observe a few instances where the beginning of an episode is characterized by relatively stationary activity which in some cases transitions to steady migration. We believe this set of observations is also described adequately as halting. The southern part of episode E6 illustrates this behavior well (Figure 7), beginning with 8 days of relatively stationary activity at ~40.075°N, followed by a steady 8 day northerly migration.

[33] The third type of behavior is “jumping” migration which refers to a temporally continuous but spatially discontinuous along-strike propagation of multiple source regions with little or no activity in between. Two clear examples of jumping migration are observed in the beginning stages of episode E3 (Figures 6 and 7). The episode begins at 41.3°N via a dense stationary cluster of activity. Over the span of a few days the level of tremor activity of this cluster diminishes, and activity jumps to the north where another dense stationary cluster of activity at 42.3°N initiates. This cluster of activity also only persists for a few days and is followed by another jump to the south where activity initiates at 40.4°N. Overall we find 10 well-defined jumps as part of four different episodes (Table 2), with a time lag between the end of ongoing activity and the initiation of new activity that ranges from -7 days (jump before activity stops) to +7 days (jump after activity stops). There is also an impressive range in jumping distances from 30 to 400 km.

[34] Previous work in northern Cascadia had also documented a single case of “gap-filling” behavior [Kao et al., 2007], which refers to a long-term relationship between ETS episodes where the lateral extent of activity in earlier episodes directly corresponds to the lateral extent of activity in a subsequent episode. The causality of this spatial rela-

tionship is relative temporally; therefore, at times it may be more appropriate to refer to this behavior as “gap forming.” Our results show evidence for this behavior when comparing the source distribution of episodes E1, E6 and E8 (Figures 6 and 7), suggesting this is not an unusual phenomenon. The lateral extent of tremor activity in episode E1 ranges from 44.5°N to 46°N which corresponds to a previously defined ETS segment [Brudzinski and Allen, 2007], whereas 13 months later episode E6 only covers the southernmost portion of the segment from 44.5°N to 45°N, forming a gap from 45°N to 46°N. The gap is filled 5 months later during episode E8, which proceeds to jump over the area active in episode E6 and continue activity south of 44.5°N. The gap-filling behavior may have implications regarding the spatial distribution and timing of future ETS activity. Analysis of subsequent tremor episodes in this region is necessary to confirm this type of relationship happens on a regular basis.

[35] Another pattern previously observed in the development of ETS activity is a “bifurcation” behavior which typically occurs as an outward propagation in opposite directions into regions absent of recent activity [e.g., Wech and Creager, 2008; Kao et al., 2009]. Our study shows evidence for this feature (episodes E4 and E8), and we also find evidence for a similar type of migration pattern we describe as “terminal convergence.” This refers to the cessation of along-strike source migration as the propagating front of activity converges into a region previously active during the episode. The final stage of episode E3 demonstrates a steady northward propagation of tremor activity from 40°N to 41.3°N and then a halting behavior as the

Table 2. Summary of Observed Jumps in NVT Activity

Event ^a	Onset of New Cluster (day of year)	Time Lag (days)	Start of New Cluster (°N)	Distance Jumped (km)
E3 (1)	136	-1	42.3	100
E3 (2)	140	+3	40.4	210
E5 (1)	305	0	41.2	180
E6 (1)	40	+7	40.9	410
E8 (1)	177	-3	45.6	30
E8 (2)	177	-3	43.7	150
E8 (3)	186	-3	40.5	300
E8 (4)	198	-1	41.5	140
E8 (5)	202	-7	40.5	110
E8 (6)	209	-5	42.1	140

^aNumbers in parentheses refer to jumps.

propagation of tremor activity terminally converges into a previously active region at 41.3°N (Figures 6 and 7). Other examples of terminal convergence can be found in episode E8 and during the northern Cascadia ETS episode in April–May 1997 [Kao *et al.*, 2009]. Although bifurcation and terminal convergence behaviors occur separately, we believe they represent similar aspects of tremor migration that demonstrate tremor activity tends to be restricted to recently inactive regions. This could be interpreted as either tremor generated by the liberation of fluids or by shear failure along a fault. In either scenario, once a region has depleted its local reservoir or relieved strain locally along the fault, it becomes difficult for the same region to be reactivated without sufficient time to acquire the critical amount of fluid or strain necessary to generate new activity.

[36] The spatial and temporal patterns of tremor activity discovered during episode E8 are the most complex along the Cascadia margin reported to date. The episode progresses from the Oregon–Washington border in mid-June to the southern end of the subduction zone by early July and then backtracks to the Klamath–Siletzia terrain boundary in southern Oregon in early August via steady migration, halting, jumping, bifurcation, and terminal convergence (Figures 6 and 7). There are six main clusters of activity ranging in length from 30 to 165 km which are separated by intermittent jumps ranging in length from 30 to 300 km. The cumulative length of activity of this episode is ~600 km which accounts for nearly 40% of the total length of activity observed during the entire 2 year study period. A potential reason for the immensity of this episode could be a fortuitous overlap of the regional ETS recurrence intervals of central and southern Cascadia, which are 19 ± 4 months and 10 ± 2 months, respectively [Brudzinski and Allen, 2007; Szeliga *et al.*, 2008].

[37] While the fact that this temporally continuous episode of NVT extends over 650 km in along-strike distance seems unusual, it does not appear to be unprecedented in this region. The single station processing of Brudzinski and Allen [2007] found there was a 2 month ETS episode at the end of 2003 that was detected at stations first in northern California, then in southern Oregon, ending in northern Oregon. The lack of instrumentation at that time limits further analysis, but it suggests migration of NVT over large regions is not simply due to coincidence. Moreover, single station processing also shows evidence for a continuous tremor episode in March–May 2008 along nearly the entire Cascadia margin (Figure S1), doubling the longest spatial extent of any episode analyzed in this study. Thus, a physical mechanism will be needed to explain how the process can migrate both continuously (~ 5 km/d) and discontinuously (jumping 30–400 km), with the latter in contrast to the steady progression implied from geodetic slip inversions [e.g., Dragert *et al.*, 2001; Melbourne *et al.*, 2005; Dragert *et al.*, 2004] and tremor source migration [e.g., Kao *et al.*, 2006; Royle *et al.*, 2006] in northern Cascadia. Finally, we notice most episodes in our study are characterized by multiple patches of activity with characteristic dimensions reminiscent of asperities in great earthquakes. As such, we hope that further analysis of both short-term complexities in nonvolcanic tremor propagation like steady migration, halting, jumping, bifurcation, and terminal convergence and long-term complexities like gap

filling can shed new light on the evolution of complex earthquake ruptures.

5. Correlation of Nonvolcanic Tremor With Slow Slip

[38] Analysis of GPS time series have documented transient deformation episodes modeled as slow slip on the plate interface that occur coincident with NVT along the Cascadia margin [e.g., Rogers and Dragert, 2003; Szeliga *et al.*, 2004; Brudzinski and Allen, 2007; Szeliga *et al.*, 2008], as well as other subduction zones like that of southwest Japan [e.g., Obara *et al.*, 2004], Mexico [Payero *et al.*, 2008; Brudzinski *et al.*, submitted manuscript, 2008] and Alaska [Ohta *et al.*, 2006; Peterson and Christensen, 2009]. In southern Cascadia, previous analysis of GPS data for transient motion is limited during the time period of our study, but single station analysis up to early 2007 can be compared with our first six episodes [Holtkamp and Brudzinski, 2010]. We find at least two GPS stations with concurrent transient motion within the region of NVT source locations for episodes E1, E4 and E6, including both the northern and southern clusters of episode E6. Unfortunately, GPS time series have not been evaluated at stations within the region of NVT locations for episodes E2, E3 and E5, limiting our ability to ascertain whether detectable slow slip occurred during these events. Recent results from Cascadia and Japan indicate that even small episodes of tremor are accompanied by collocated transient slip visible on strainmeters or tiltmeters [e.g., Obara *et al.*, 2004; Wang *et al.*, 2008], suggesting that our spatial and temporal distribution of tremor epicenters likely corresponds to the distribution of slow slip along the plate interface. We envision a more thorough investigation of the relationship between tremor and slow slip in southern Cascadia will be possible now that the EarthScope Plate Boundary Observatory has been deployed.

6. Along-Strike Segmentation

[39] Although evidence for tremor and slip have been found throughout the full extent of the Cascadia margin over the past 10 years, episodes do not typically occur along the entire length of the margin at the same time [Brudzinski and Allen, 2007; Szeliga *et al.*, 2008; Holtkamp and Brudzinski, 2010]. Previous studies have defined apparent ETS segmentation where ETS episodes recur over roughly the same location without much activity in neighboring regions as well as some indications of repeating initiation and termination points of tremor propagation. Brudzinski and Allen [2007] investigated the along-strike extent of 22 ETS episodes between 1997 and 2006 in southern Cascadia and defined three segment boundaries based on the extent of NVT activity seen on individual stations. Holtkamp and Brudzinski [2010] found six additional episodes consistent with this segmentation by including additional stations and extending the study into 2007. We adopt the segmentation nomenclature of Holtkamp and Brudzinski [2010], where long-standing segments and potential subsegments are assigned a numeric and alphabetic character, respectively, increasing in value from south to north (Figure 1c).

[40] In our study, we investigate segmentation boundaries in two ways. First, we determine boundaries where the

initiation and termination of continuous tremor migration are consistent and repeatable features. With this approach, the three segment boundaries proposed in earlier work are reaffirmed by our more detailed study of nonvolcanic tremor source migration. In fact, only one of our eight NVT episodes shows any evidence that tremor migrates across a previously defined segment boundary, but the exception is the complex episode E8 where tremor migration halts as it crosses the boundary and proceeds to terminally converge at the boundary.

[41] A second approach to support our initially defined segmentation boundaries is by comparing them with patterns in the along-strike density of tremor locations within and between NVT episodes (Figures 7 and S2). It is worth noting that a lull in tremor density is observed near 44°N, but this feature is likely an artifact of the limited station coverage during episode E2 as TA sites arrived late in southern Oregon (Figure 6). In all other cases, prominent lulls in along-strike tremor activity correspond well with the location of the segment boundaries determined by tremor initiation and termination.

[42] Considering there is evidence for these three boundaries being persistent over the 10 years of recording, it supports the notion the configuration of the ETS segmentation is a long-standing feature. This is particularly important in light of the observation that the ETS segments occur immediately landward from the proposed locations of asperities on the Cascadia megathrust (Figure 1c) [Brudzinski and Allen, 2007]. The asperity locations are based on large, low-gravity, sedimentary basins in the fore arc interpreted to indicate seismogenic segmentation, derived from global surveys finding most megathrust earthquake moment and high coseismic slip occur beneath the fore-arc basins from gravity, bathymetry, and seismic profiling [e.g., Song and Simons, 2003; Wells et al., 2003]. The apparent correlation between segmentation of the seismogenic zone and segmentation of the ETS zone suggests that the conditions that promote locking (or lack thereof) on the megathrust also influence the ETS zone.

[43] A study examining fore-arc structure and rupture propagation of great earthquakes also finds a correlation between fore-arc gravity variations and the boundaries of great earthquake ruptures, which requires that long-lived, upper plate structural/geological heterogeneity is a first-order control on along-strike rupture extent [Llenos and McGuire, 2007]. In fact, patches of velocity-strengthening material appear to prevent large throughgoing ruptures and represent a primary cause of megathrust segmentation. Considering the correlation between megathrust and ETS segmentation, we hypothesize that areas of the transition zone with little coupling could represent barriers to ETS migration. There may be some evidence to support this if prominent lulls in along-strike tremor activity at the ETS segment boundaries indicate these areas slip more freely between episodes.

[44] Our analysis of NVT source locations reveals some additional migration initiation and termination points that were not apparent from previous investigation (dotted lines in Figures 1c and 7). These locations are also associated with lulls in along-strike tremor density during the 2 years of our study (Figure S2). The additional segment boundaries do not necessarily correspond to the edges of fore-arc basins

thought to represent long-term megathrust asperities. However, the limited time frame makes it difficult to determine whether these subsegment boundaries are short-term or long-lived features. For example, the subsegments proposed in regions 2 and 3 are only determined by the division between two sequential episodes, which may just represent gap-filling behavior. Using earthquake behavior as a guide, it may be that the subsegment behavior represents dynamic heterogeneity due to the low-stress regions leftover from past ruptures [Shaw, 2000], where the locations of these dynamic heterogeneities vary on the scale of an earthquake cycle. Perhaps the most likely boundary to persist is boundary 1b–1c (Figure 1c) between the northernmost and central subsegments of region 1 which does correspond with the edge of the southernmost offshore fore-arc basin, as well as where there is a prominent 50 km wide gap in tremor activity with very few source locations despite a very active region just to the north. Additional analysis of future ETS episodes will be necessary to see whether these lulls, gaps, and subsegment divisions persist.

7. Low-Frequency Earthquakes

[45] Nonvolcanic tremor was originally recognized as an emergent, low-amplitude semicontinuous seismic signal enriched in the frequency passband from 2 to 8 Hz and depleted in the higher-frequency passband from 10 to 20 Hz of similar magnitude earthquakes [e.g., Obara, 2002]. In southwest Japan, accompanying much of the tremor signal are relatively energetic and isolated bursts with identifiable body waves that have been referred to as low-frequency earthquakes [Shelly et al., 2006]. In this case, NVT has been shown to be the manifestation of repeatable low-frequency earthquake swarms of activity occurring along the deeper extensions of the plate interface [Shelly et al., 2007a; Brown et al., 2008].

[46] During the visual inspection stage of our semi-automated analysis of NVT, we identified distinct and isolated bursts usually occurring during quiescent periods of tremor activity that we interpret to be low-frequency earthquakes in Cascadia. Figure 2c shows stacked envelope seismograms for an example of this type of burst detected using our semiautomated routine. Visual analysis of the corresponding raw seismograms filtered between 2 and 6 Hz provide an opportunity to identify arrivals of both P and S waves that produce a source location within 5 km of the hypocenter determined using the stacked envelope seismogram arrivals (Figure 2e). For all LFEs we identified, the corresponding source locations fall within the band of NVT and is coincident with the along-strike progression in tremor migration (Figure 7).

[47] As in southwest Japan, the spectral characteristics of LFEs in Cascadia are distinguished from smaller magnitude earthquakes (Figure 3). Both LFE and NVT spectra are enriched at 1–4 Hz with a rapid dropoff at higher frequencies. Further inspection of earthquake catalogs shows no indication of any local or teleseismic activity that corresponds with the events we identify as LFEs.

[48] In total, we detect 128 LFE events through visual identification of distinct bursts in envelope and filtered seismograms and confirmation through comparison with spectrograms and earthquake catalogs. This approach results

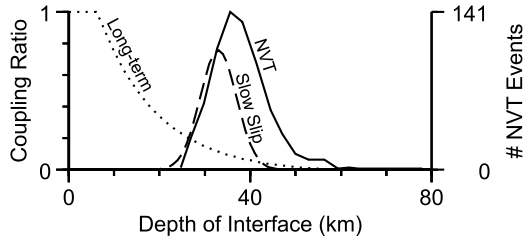


Figure 8. Distribution of NVT and coupling ratios versus depth of the plate interface. Dotted line represents the interseismic coupling ratio from McCaffrey *et al.* [2007]. Dashed line represents additional coupling necessary between ETS events to produce slow slip episodes across Cascadia [Holtkamp and Brudzinski, 2010]. Solid line corresponds to a histogram of NVT epicenters in southern Cascadia projected onto the plate interface binned per kilometer and smoothed.

in an uneven along-strike distribution of LFE activity when compared to the more continuous belt of NVT activity (Figure 7). LFEs we identify occur most prominent in dense clusters throughout the southern half of our study region, but do also occur diffusely elsewhere. Comparison of LFE waveforms from the dense clusters with that in other regions suggest that the level of ongoing tremor is less in these regions, allowing for easier visual detection of LFEs. We do not see a significant difference in average amplitude between LFE and NVT (Figure 3). This supports the notion that LFEs appear as prominent bursts due more to the reduced background level of tremor than to larger magnitude of the LFE source.

[49] Our results indicate that low-frequency earthquakes are not restricted to southwest Japan and that NVT in Cascadia may also be composed of a swarm of LFEs [i.e., Shelly *et al.*, 2007a]. Although lower station density prohibits a comparable study to that in Japan, correlation of the detected LFE waveforms with the remaining time series and autocorrelation for the detection of other LFEs should be the subject of future study.

8. Relationship of Nonvolcanic Tremor to Interplate Coupling Structure

[50] Understanding variations in the degree of interplate coupling is central to understanding how ETS relates to the seismogenic potential. In Cascadia, geodetic inversions of interseismic GPS motions model the fully locked portion of the plate interface extending to a depth of 7 km, followed by a monotonic decrease that leaves only ~10% coupling at depths of 30–40 km (dotted line in Figure 8) [Wang *et al.*, 2003; McCaffrey *et al.*, 2007]. Moreover, long-term tidal and leveling records indicate that the edge of interseismic coupling only extends down to 15–25 km depth in our study region [Burgette *et al.*, 2009] (Figure 1a). Meanwhile, a Gaussian-like distribution of NVT locations are clustered at ~37 km depth, which raises the question why tremor is occurring in an area of such low coupling if faulting on the interface is responsible for NVT (solid line in Figure 8). Analysis of slow slip events in Cascadia show they are also occurring in this depth range [Dragert *et al.*, 2004; Szeliga

et al., 2008], demonstrating that a significant amount of fault slip is present. Analysis of GPS motions between ETS episodes find the best fitting model for interface coupling ratio over the past ~10 years has an increase reaching nearly 80% at ~33 km depth (dashed line in Figure 8) [Holtkamp and Brudzinski, 2010]. We do not dismiss the slight offset between slow slip and NVT source zones considering there are even larger offsets observed in Mexico [Payero *et al.*, 2008; Song *et al.*, 2009; Brudzinski *et al.*, submitted manuscript, 2008].

[51] In any case, there is a definitive offset from the zone of long-term coupling shallower than 15–25 km depth [Burgette *et al.*, 2009] to the slow slip and NVT that occur associated in the 30–40 km depth range, laterally separated by as much as 50 km (Figure 1a). We believe this is important in terms of hazards in Cascadia, as it indicates the ETS zone does not abut the region of strong coupling on the plate interface. Characterizing the proximity of the locked portion of the plate interface to the ETS zone is fundamental when addressing potential relationships between ETS and updip seismogenesis, including two key questions: (1) Can updip stress loading during an ETS episode trigger megathrust earthquakes? (2) Can coseismic slip propagate into the ETS zone during the next great earthquake?

[52] The northern Cascadia ETS zone appears to abut the downdip extent of the thermally and geodetically defined transition zone, such that updip stress perturbations associated with slow slip could conceivably increase the likelihood for failure of the locked zone [e.g., Dragert *et al.*, 2004; Mazzotti and Adams, 2004]. Additionally, the downdip edge of the ETS zone may more precisely delineate the onset of free slip behavior along the megathrust, potentially extending the zone of coseismic failure during a great earthquake at least 50 km further inland beneath population centers of the Pacific Northwest if short-term strain accumulation during the ETS cycle is conditionally stable and can be released seismogenically. Conversely, the large spatial offset between the thermally and geodetically defined transition zone and the southern Cascadia ETS zone may be the manifestation of two separated long-term and short-term locking zones where the transition from brittle-ductile behavior is more complex. Under this scenario, the efficiency of stress transmission and slip propagation through a weakly coupled regime in between would determine how well the two locking zones communicate during either seismogenic or transient deformation episodes.

9. Conclusions

[53] We studied in detail eight NVT episodes which occurred between November 2005 and August 2007 throughout the southern half of the Cascadia subduction zone. We developed a semiautomated location algorithm to detect the most prominent bursts of energy within extended duration tremor sequences and invert visually inspected relative arrival times for source locations. We detect distinct, isolated bursts of energy within the tremor similar to observations from southwest Japan that we also term low-frequency earthquakes. In total, over 1100 NVT bursts and over 125 LFE events were cataloged by thoroughly analyzing the most active nighttime hour per day for each

tremor episode, as a means of providing overall constraints on tremor distribution and migration patterns.

[54] The epicentral locations of all well constrained tremors occur within a narrow belt which is bounded by the surface projections of the 30 and 40 km contours of the subducting plate interface. This geographic distribution produces an intriguing spatial anticorrelation between local seismicity and NVT, suggesting a mutually exclusive relationship. We propose that the combination of high pore fluid pressures and the transition in frictional behavior in the ETS zone favor tremor generation instead of interplate seismicity, while frequent ETS activity produces a semicontinuous relaxation of strain within the overriding and subducting plates that further inhibit seismicity surrounding the ETS source region.

[55] Our belt-like distribution of tremor epicenters is ~50 km inland from the 450°C isotherm on the plate interface, while in northern Cascadia the zone of NVT abuts this isotherm, indicating that NVT does not appear at a precise temperature. It is perhaps surprising that NVT is spatially separated from the thermally and geodetically defined end of the seismogenic transition zone, which could limit both the downdip propagation of coseismic slip associated with the next great earthquake and potential updip triggering of earthquakes by ETS.

[56] Along-strike patterns in NVT source propagation during the eight NVT episodes analyzed are complex as seen in short-term steady, halting, jumping, bifurcation, terminal convergence and long-term gap-filling migration patterns. The initiation and termination of tremor activity within and between NVT episodes complement the three previously defined segment boundaries of Brudzinski and Allen [2007], supporting the hypothesis of along-strike segmentation in ETS, which may be related to segmentation of the megathrust.

[57] **Acknowledgments.** Our analysis relied heavily on seismic data from the PNSN, BDSN, GSN, PBO, and OATS obtained via the IRIS DMC. We benefited from discussions with R. Allen, K. Creager, Y. Dilek, W. Hart, H. Hinojosa, H. Kao, H. Mix, R. Porritt, D. Schmidt, S. Sit, and A. Wech. H. Kao, A. Wech, and an anonymous reviewer provided beneficial comments which significantly improved our manuscript. This project is supported by the National Science Foundation grant EAR-0642765.

References

- Aguiar, A. C., T. I. Melbourne, and C. Scrivner (2007), Tremor constraints on moment release during the 2007 ETS from surface and borehole seismometers, *Eos Trans. AGU*, 88(52), Fall Meet. Suppl., Abstract T13F-03.
- Audet, P., M. G. Bostock, N. I. Christensen, and S. M. Peacock (2009), Seismic evidence for overpressured subducted oceanic crust and megathrust fault sealing, *Nature*, 457, 76–78.
- Audet, P., M. G. Bostock, D. C. Boyarko, M. R. Brudzinski, and R. M. Allen (2010), Slab morphology in the Cascadia fore arc and its relation to episodic tremor and slip, *J. Geophys. Res.*, 115, B00A16, doi:10.1029/2008JB006053.
- Bostock, M. G., R. D. Hyndman, S. Rondenay, and S. M. Peacock (2002), An inverted continental Moho and serpentization of the forearc mantle, *Nature*, 417, 536–538, doi:10.1038/417536a.
- Boyarko, D. C., and M. R. Brudzinski (2007), Spatial and temporal patterns of non-volcanic tremor source locations all along the Cascadia subduction zone, *Eos Trans. AGU*, 88(52), Fall Meet. Suppl., Abstract T21A-0345.
- Brown, J. R., G. C. Beroza, and D. R. Shelly (2008), An autocorrelation method to detect low frequency earthquakes within tremor, *Geophys. Res. Lett.*, 35, L16305, doi:10.1029/2008GL034560.
- Brudzinski, M. R., and R. M. Allen (2007), Segmentation in episodic tremor and slip all along Cascadia, *Geology*, 35, 907–910, doi:10.1130/G23740A.1.
- Brudzinski, M., E. Cabral-Cano, F. Correa-Mora, C. DeMets, and B. Márquez-Azúa (2007), Slow slip transients along the Oaxaca subduction segment from 1993 to 2007, *Geophys. J. Int.*, 171, 523–538, doi:10.1111/j.1365-246X.2007.03542.x.
- Burgette, R. J., R. J. Weldon II, and D. A. Schmidt (2009), Interseismic uplift rates for western Oregon and along-strike variation in locking on the Cascadia subduction zone, *J. Geophys. Res.*, 114, B01408, doi:10.1029/2008JB005679.
- Delahaye, E. J., J. Townend, M. E. Reyners, and G. Rogers (2009), Microseismicity but no tremor accompanying slow slip in the Hikurangi subduction zone, New Zealand, *Earth Planet. Sci. Lett.*, 277, 21–28, doi:10.1016/j.epsl.2008.09.038.
- Dragert, H., K. L. Wang, and T. S. James (2001), A silent slip event on the deeper Cascadia subduction interface, *Science*, 292, 1525–1528, doi:10.1126/science.1060152.
- Dragert, H., G. C. Rogers, J. Cassidy, H. H. Kao, and K. Wang (2004), Episodic tremor and slip in northern Cascadia, *Prog. Rep. 04HQGR0047*, pp. 1–6, U.S. Geol. Surv., Reston, Va.
- Efron, B. (1979), Bootstrap methods: Another look at the jackknife, *Ann. Stat.*, 7, 1–26, doi:10.1214/aos/1176344552.
- Fay, N. P., and E. D. Humphreys (2008), Forces acting on the Sierra Nevada block and implications for the strength of the San Andreas fault system and the dynamics of continental deformation in the western United States, *J. Geophys. Res.*, 113, B12415, doi:10.1029/2008JB005809.
- Hermann, R. B. (2004), Computer programs in seismology: Version 3.30, Saint Louis Univ., Saint Louis, Mo.
- Holtkamp, S., and M. R. Brudzinski (2010), Determination of slow slip episodes and strain accumulation along the Cascadia margin, *J. Geophys. Res.*, 115, B00A17, doi:10.1029/2008JB006058.
- Hyndman, R. D., and K. Wang (1993), Thermal constraints on the zone of major thrust earthquake failure: The Cascadia subduction zone, *J. Geophys. Res.*, 98, 2039–2060, doi:10.1029/92JB02279.
- Hyndman, R. D., and K. Wang (1995), The rupture zone of Cascadia great earthquakes from current deformation and the thermal regime, *J. Geophys. Res.*, 100, 22, 133–22,154, doi:10.1029/95JB01970.
- Ide, S., D. R. Shelly, and G. C. Beroza (2007), Mechanism of deep low frequency earthquakes: Further evidence that deep non-volcanic tremor is generated by shear slip on the plate interface, *Geophys. Res. Lett.*, 34, L03308, doi:10.1029/2006GL028890.
- Kao, H., and S.-J. Shan (2004), The source-scanning algorithm: Mapping the distribution of seismic sources in time and space, *Geophys. J. Int.*, 157, 589–594, doi:10.1111/j.1365-246X.2004.02276.x.
- Kao, H., S.-J. Shan, H. Dragert, G. Rogers, J. F. Cassidy, and K. Ramachandran (2005), A wide depth distribution of seismic tremors along the northern Cascadia margin, *Nature*, 436, 841–844, doi:10.1038/nature03903.
- Kao, H., S.-J. Shan, H. Dragert, G. Rogers, J. F. Cassidy, K. Wang, T. S. James, and K. Ramachandran (2006), Spatial-temporal patterns of seismic tremors in northern Cascadia, *J. Geophys. Res.*, 111, B03309, doi:10.1029/2005JB003727.
- Kao, H., S.-J. Shan, G. Rogers, and H. Dragert (2007), Migration characteristics of seismic tremors in the northern Cascadia margin, *Geophys. Res. Lett.*, 34, L03304, doi:10.1029/2006GL028430.
- Kao, H., S.-J. Shan, H. Dragert, and G. Rogers (2009), Northern Cascadia episodic tremor and slip: A decade of observations from 1997 to 2007, *J. Geophys. Res.*, 114, B00A12, doi:10.1029/2008JB006046.
- Kodaira, S., T. Iidaka, A. Kato, J. O. Park, T. Iwasaki, and Y. Kaneda (2004), High pore fluid pressure may cause silent slip in the Nankai Trough, *Science*, 304, 1295–1298, doi:10.1126/science.1096535.
- La Rocca, M., W. McCausland, D. Galluzzo, S. Malone, G. Saccorotti, and E. Del Pezzo (2005), Array measurements of deep tremor signals in the Cascadia subduction zone, *Geophys. Res. Lett.*, 32, L21319, doi:10.1029/2005GL023974.
- La Rocca, M., K. C. Creager, D. Galluzzo, S. Malone, J. E. Vidale, J. R. Sweet, and A. G. Wech (2009), Cascadia tremor located near plate interface constrained by *S* minus *P* wave times, *Science*, 323, 620–623, doi:10.1126/science.1167112.
- Liu, Y., and J. R. Rice (2005), Aseismic slip transients emerge spontaneously in three-dimensional rate and state modeling of subduction earthquake sequences, *J. Geophys. Res.*, 110, B08307, doi:10.1029/2004JB003424.
- Liu, Y., and J. R. Rice (2007), Spontaneous and triggered aseismic deformation transients in a subduction fault model, *J. Geophys. Res.*, 112, B09404, doi:10.1029/2007JB004930.
- Llenos, A. L., and J. J. McGuire (2007), Influence of fore-arc structure on the extent of great subduction zone earthquakes, *J. Geophys. Res.*, 112, B09301, doi:10.1029/2007JB004944.

- Lohman, R. B., and J. J. McGuire (2007), Earthquake swarms driven by aseismic creep in the Salton Trough, California, *J. Geophys. Res.*, **112**, B04405, doi:10.1029/2006JB004596.
- Ludwin, R. S., A. I. Qamar, S. D. Malone, C. Jonientz-Trisler, R. S. Crosson, R. Benson, and S. C. Moran (1994), Earthquake hypocenters in Washington and northern Oregon, 1987–1989, *Inf. Circ.* **89**, 40 pp., Wash. State Dep. of Nat. Resour., Olympia.
- Matsubara, M., K. Obara, and K. Kasahara (2009), High-V_p/V_s zone accompanying non-volcanic tremors and slow-slip events beneath southwestern Japan, *Tectonophysics*, **472**, 6–17, doi:10.1016/j.tecto.2008.06.013.
- Mazzotti, S., and J. Adams (2004), Variability of near-term probability for the next great earthquake on the Cascadia subduction zone, *Bull. Seismol. Soc. Am.*, **94**, 1954–1959, doi:10.1785/012004032.
- McCaffrey, R., A. I. Qamar, R. W. King, R. Wells, G. Khazaradze, C. A. Williams, C. W. Stevens, J. J. Vollick, and P. C. Zwick (2007), Fault locking, block rotation and crustal deformation in the Pacific Northwest, *Geophys. J. Int.*, **169**, 1315–1340, doi:10.1111/j.1365-246X.2007.03371.x.
- McCaffrey, R., L. M. Wallace, and J. Beavan (2008), Slow slip and frictional transition at low temperature at the Hikurangi subduction zone, *Nat. Geosci.*, **1**, 316–320, doi:10.1038/ngeo178.
- McCauley, W., S. Malone, and D. Johnson (2005), Temporal and spatial occurrence of deep non-volcanic tremor: From Washington to northern California, *Geophys. Res. Lett.*, **32**, L24311, doi:10.1029/2005GL024349.
- McCrory, P. A., J. L. Blair, D. H. Oppenheimer, and S. R. Walter (2004), Depth to the Juan de Fuca slab beneath the Cascadia subduction margin—A 3-D model for sorting earthquakes, *Data Ser. 91*, U.S. Geol. Surv., Reston, Va. (Available at <http://pubs.usgs.gov/ds/91/>.)
- Melbourne, T. I., W. M. Szeliga, M. M. Miller, and V. M. Santillan (2005), Extent and duration of the 2003 Cascadia slow earthquake, *Geophys. Res. Lett.*, **32**, L04301, doi:10.1029/2004GL021790.
- Obara, K. (2002), Nonvolcanic deep tremor associated with subduction in southwest Japan, *Science*, **296**, 1679–1681, doi:10.1126/science.1070378.
- Obara, K., H. Hirose, F. Yamamizu, and K. Kasahara (2004), Episodic slow slip events accompanied by non-volcanic tremors in southwest Japan subduction zone, *Geophys. Res. Lett.*, **31**, L23602, doi:10.1029/2004GL020848.
- Ohta, Y., J. T. Freymueller, S. Hreinsdóttir, and H. Suito (2006), A large slow slip event and the depth of the seismogenic zone in the south central Alaska subduction zone, *Earth Planet. Sci. Lett.*, **247**, 108–116, doi:10.1016/j.epsl.2006.05.013.
- Oppenheimer, D., et al. (1993), The Cape Mendocino, California earthquakes of April 1992: Subduction at the triple junction, *Science*, **261**, 433–438, doi:10.1126/science.261.5120.433.
- Ozawa, S., H. Suito, and M. Tobita (2007), Occurrence of quasi-periodic slow-slip off the east coast of the Boso peninsula, central Japan, *Earth Planets Space*, **59**, 1241–1245.
- Payero, J. S., V. Kostoglodov, N. Shapiro, T. Mikumo, A. Iglesias, X. Pérez-Campos, and R. W. Clayton (2008), Nonvolcanic tremor observed in the Mexican subduction zone, *Geophys. Res. Lett.*, **35**, L07305, doi:10.1029/2007GL032877.
- Peters, R., B. Jaffe, and G. Gelfenbaum (2007), Distribution and sedimentary characteristics of tsunami deposits along the Cascadia margin of western North America, *Sediment. Geol.*, **200**, 372–386, doi:10.1016/j.sedgeo.2007.01.015.
- Peterson, C. L., and D. H. Christensen (2009), Possible relationship between nonvolcanic tremor and the 1998–2001 slow slip event, south central Alaska, *J. Geophys. Res.*, **114**, B06302, doi:10.1029/2008JB006096.
- Rogers, G., and H. Dragert (2003), Episodic tremor and slip on the Cascadia subduction zone: The chatter of silent slip, *Science*, **300**, 1942–1943, doi:10.1126/science.1084783.
- Royle, G. T., A. J. Calvert, and H. Kao (2006), Observations of non-volcanic tremor during the northern Cascadia slow-slip event in February 2002, *Geophys. Res. Lett.*, **33**, L18313, doi:10.1029/2006GL027316.
- Rubinstein, J. L., J. E. Vidale, J. Gomberg, P. Bodin, K. C. Creager, and S. D. Malone (2007), Non-volcanic tremor driven by large transient shear stresses, *Nature*, **448**, 579–582, doi:10.1038/nature06017.
- Rubinstein, J. L., M. La Rocca, J. E. Vidale, K. C. Creager, and A. G. Wech (2008), Tidal modulation of nonvolcanic tremor, *Science*, **319**, 186–189, doi:10.1126/science.1150558.
- Rubinstein, J. L., J. Gomberg, J. E. Vidale, A. G. Wech, H. Kao, K. C. Creager, and G. Rogers (2009), Seismic wave triggering of nonvolcanic tremor, episodic tremor and slip, and earthquakes on Vancouver Island, *J. Geophys. Res.*, **114**, B00A01, doi:10.1029/2008JB005875.
- Schwartz, S. Y., and J. M. Rokosky (2007), Slow slip events and seismic tremor at circum-Pacific subduction zones, *Rev. Geophys.*, **45**, RG3004, doi:10.1029/2006RG000208.
- Segall, P., and J. R. Rice (1995), Dilatancy, compaction, and slip instability of a fluid-infiltrated fault, *J. Geophys. Res.*, **100**, 22,155–22,171, doi:10.1029/95JB02403.
- Segall, P., E. K. Desmarais, D. Shelly, A. Miklius, and P. Cervelli (2006), Earthquakes triggered by silent slip events on Kilauea volcano, Hawaii, *Nature*, **442**, 71–74, doi:10.1038/nature04938.
- Shaw, B. E. (2000), The edges of large earthquakes and the epicenters of future earthquakes: Stress-induced correlations in elastodynamic fault models, *Pure Appl. Geophys.*, **157**, 2149–2164.
- Shelly, D. R., G. C. Beroza, S. Ide, and S. Nakamura (2006), Low-frequency earthquakes in Shikoku, Japan, and their relationship to episodic tremor and slip, *Nature*, **442**, 188–191, doi:10.1038/nature04931.
- Shelly, D. R., G. C. Beroza, and S. Ide (2007a), Non-volcanic tremor and low-frequency earthquake swarms, *Nature*, **446**, 305–307, doi:10.1038/nature05666.
- Shelly, D. R., G. C. Beroza, and S. Ide (2007b), Complex evolution of transient slip derived from precise tremor locations in western Shikoku, Japan, *Geochem. Geophys. Geosyst.*, **8**, Q10014, doi:10.1029/2007GC001640.
- Song, T.-R. A., and M. Simons (2003), Large trench-parallel gravity variations predict seismogenic behavior in subduction zones, *Science*, **301**, 630–633, doi:10.1126/science.1085557.
- Song, T.-R. A., D. V. Helmberger, M. R. Brudzinski, R. W. Clayton, P. Davis, X. Pérez-Campos, and S. K. Singh (2009), Subducting slab ultra-slow velocity layer coincident with silent earthquakes in southern Mexico, *Science*, **324**, 502–506.
- Szeliga, W., T. I. Melbourne, M. M. Miller, and V. M. Santillan (2004), Southern Cascadia episodic slow earthquakes, *Geophys. Res. Lett.*, **31**, L16602, doi:10.1029/2004GL020824.
- Szeliga, W., T. Melbourne, M. Santillan, and M. Miller (2008), GPS constraints on 34 slow slip events within the Cascadia subduction zone, 1997–2005, *J. Geophys. Res.*, **113**, B04404, doi:10.1029/2007JB004948.
- Trehu, A. M., J. Braumiller, and J. L. Nabelek (2008), Probable low-angle thrust earthquakes on the Juan de Fuca–North America plate boundary, *Geology*, **36**, 127–130, doi:10.1130/G24145A.1.
- Wang, K., and G. C. Rogers (1994), An explanation for the double seismic layers north of the Mendocino Triple Junction, *Geophys. Res. Lett.*, **21**, 121–124, doi:10.1029/93GL03538.
- Wang, K., R. Wells, S. Mazzotti, R. D. Hyndman, and T. Sagiya (2003), A revised dislocation model of interseismic deformation of the Cascadia subduction zone, *J. Geophys. Res.*, **108**(B1), 2026, doi:10.1029/2001JB001227.
- Wang, K., H. Dragert, H. Kao, and E. Roeloffs (2008), Characterizing an “uncharacteristic” ETS event in northern Cascadia, *Geophys. Res. Lett.*, **35**, L15303, doi:10.1029/2008GL034415.
- Wech, A. G., and K. C. Creager (2008), Automated detection and location of Cascadia tremor, *Geophys. Res. Lett.*, **35**, L20302, doi:10.1029/2008GL035458.
- Wells, R. E., R. J. Blakely, Y. Sugiyama, D. W. Scholl, and P. A. Dinterman (2003), Basin-centered asperities in great subduction zone earthquakes: A link between slip, subsidence, and subduction erosion?, *J. Geophys. Res.*, **108**(B10), 2507, doi:10.1029/2002JB002072.
- Williams, T. B., H. M. Kelsey, and J. T. Freymueller (2006), GPS-derived strain in northwestern California: Termination of the San Andreas fault system and convergence of the Sierra Nevada–Great Valley block contribute to southern Cascadia forearc contraction, *Tectonophysics*, **413**, 171–184, doi:10.1016/j.tecto.2005.10.047.
- Yoshida, S., and N. Kato (2003), Episodic aseismic slip in a two-degree-of-freedom block-spring model, *Geophys. Res. Lett.*, **30**(13), 1681, doi:10.1029/2003GL017439.
- Yoshioka, S., and K. Murakami (2007), Temperature distribution of the upper surface of the subducted Philippine Sea Plate along the Nankai Trough, southwest Japan, from a three-dimensional subduction model: Relation to large interplate and low-frequency earthquakes, *Geophys. J. Int.*, **171**, 302–315, doi:10.1111/j.1365-246X.2007.03510.x.

D. C. Boyarko and M. R. Brudzinski, Department of Geology, Miami University, Oxford, OH 45056, USA. (brudzimr@muohio.edu)